Imaging chlorophyll fluorescence with an airborne narrow-band multispectral camera for vegetation stress detection

P.J. Zarco-Tejada [a,*], J.A.J. Berni [a], L. Suárez [a], G. Sepulcre-Cantó [a], F. Morales [b], J.R. Miller [c]

[a] Instituto de Agricultura Sostenible (IAS), Consejo Superior de Investigaciones Científicas (CSIC), Córdoba, Spain
[b] Departamento de Nutrición Vegetal, Estación Experimental de Aula Dei (EEAD), Consejo Superior de Investigaciones Científicas (CSIC), Apdo, 13034, 50080 Zaragoza, Spain
[c] Dept. of Earth and Space Science and Engineering, York University, Toronto, Canada

ARTICLE INFO

ABSTRACT

Progress in assessing the feasibility for imaging fluorescence using the O_2-A band with 1 nm full-width half-maximum (FWHM) bands centered at 757.5 and 760.5 nm is reported in this paper. Multispectral airborne data was acquired at 150 m above ground level in the thermal, visible and near infrared regions yielding imagery at 15 cm spatial resolution. Simultaneous field experiments conducted in olive, peach, and orange orchards (water stress trials), and an olive orchard (variety trial) enabled the detected variability in fluorescence emission to be examined as function of stress status. In a parallel modelling activity the coupled leaf–canopy reflectance–fluorescence model, FluorMOD, was used to assess fluorescence retrieval capability by the *in-filling* method, as well as by fluorescence indices from the published literature. Fluorescence retrievals using the *in-filling* method, the derivative index D702/D680 and reflectance indices R690/R630, R761−R757, and R761/R757 yielded the best results in the simulation study, while demonstrating insensitivity to leaf area index (LAI) variation. The fluorescence *in-filling* method, derivative index D702/D680, and R761−R757 were the indices least affected by chlorophyll $a + b$ (Cab) variation. On the other hand, other published indices for fluorescence detection at leaf and canopy levels exhibited high sensitivity to variations in Cab and LAI, and therefore were considered less suitable for in-field fluorescence detection. The fluorescence signal extraction from airborne imagery using the *in-filling* method was validated through comparisons with field-measured steady-state fluorescence (*Fs*) using the PAM-2100 and GFS-3000 instruments, confirming simulation predictions. The water stress experiments conducted on olive and peach orchards demonstrated the feasibility of chlorophyll fluorescence (*F*) extraction at the tree level from the airborne imagery, yielding determination coefficients $r^2 = 0.57$ (olive), and $r^2 = 0.54$ (peach). Consistent results were obtained between airborne *F* and ground truth assimilation (*A*) measured in the olive variety field experiment under no water stress levels, yielding $r^2 = 0.71$.

1. Introduction

The early detection of water stress has been long identified as critical to avoid yield losses in crops, which can be affected even by short-term water stress deficits (Hsiao et al., 1976). Water stress is developed in crops when the evaporative demand exceeds the supply of water from the soil (Slatyer, 1967). A remote sensing indicator for water stress detection was successfully demonstrated in the seventies with near-field thermal infrared radiation (Idso et al., 1978, 1981; Jackson et al., 1977, 1981; Jackson & Pinter, 1981) and more recently with high-resolution airborne thermal imagers flown over orchard crops (Sepulcre-Cantó et al., 2006, 2007). The successful detection of water stress using the thermal region is in response to the canopy transpiration changes, where canopy temperature increases with reductions in evaporative cooling.

In addition to canopy temperature, other physiological and structural indicators have been proposed for remote sensing detection of water stress, such as wilting (Bradford & Hsiao, 1982), loss of leaf area (Bradford & Hsiao, 1982; Wolfe et al., 1983) and chlorophyll content (Björkman & Powles, 1984). Leaf water content is proposed as the amount of water per unit leaf area, and remote sensing indices such as a water band index (WBI) (Peñuelas et al., 1993, 1997), a moisture stress index (MSI) (Rock et al., 1986) or the normalized difference water index (NDWI) (Gao, 1996) have been shown to track water content at the canopy level. Nevertheless, changes in leaf water content only occur at advanced stages of dehydration in many (but not all) species, therefore representing a parameter of limited interest for predicting crop water status. A more valuable goal is to develop *pre-visual* indicators of stress, i.e. before the onset of severe stress. Suggested *pre-visual* indicators of stress are the physiological reflectance index (PRI) which is sensitive to

* Corresponding author. Instituto de Agricultura Sostenible (IAS), Consejo Superior de Investigaciones Científicas (CSIC), Alameda del Obispo, s/n, 14004–Córdoba, Spain. Tel.: +34 957 499 280, +34 676 954 937; fax: +34 957 499 252.
E-mail address: pzarco@ias.csic.es (P.J. Zarco-Tejada).
URL: http://www.ias.csic.es/pzarco (P.J. Zarco-Tejada).

xanthophyll pigment detection under water stress conditions (Peguero-Pina et al., 2008; Suarez et al., 2008; Suárez et al., 2009; Thenot et al., 2002), and solar-induced chlorophyll fluorescence emission (Flexas et al., 1999, 2000, 2002; Moya et al., 2004) due to the strong correlation demonstrated between steady-state chlorophyll fluorescence Fs and stomatal conductance. In addition, several studies have assessed the relationship of chlorophyll fluorescence with photosynthesis and plant physiological status (Krause & Weis, 1984; Lichtenthaler & Rinderle, 1988; Lichtenthaler, 1992; Larcher, 1994; Papageorgiou, 1975; Schreiber & Bilger, 1987; Schreiber et al., 1994). Fv/Fm, Φ_{PSII} (Yield), qP, Φ_{exc}, and NPQ (or qN) are the chlorophyll fluorescence parameters most frequently used to characterize the functioning of the photosynthetic apparatus under non-stress and stress conditions (see Morales et al., 1991, 1998, 2000; and Abadía et al., 1999 and Morales et al., 2006 for reviews). Although comparatively steady-state chlorophyll fluorescence Fs has received much less attention, its potential importance for chlorophyll fluorescence detection using remote sensing methods has been recently emphasized (Soukupová et al., 2008), along with increasing scientific interest during the past five years.

Several publications have described reflectance indices potentially related to incremental effects of fluorescence emission as an addition to leaf and canopy reflected signal. In particular, indices related to fluorescence emission bands at 685 and 740 nm have been proposed to assess the relationship between apparent reflectance and chlorophyll fluorescence at both leaf and canopy levels (Zarco-Tejada et al., 2000a,b), while attempting to minimize structural effects and chlorophyll content sensitivity to thereby derive robust fluorescence indices.

At the laboratory level, results in diurnal studies have shown that optical indices R680/R630, R685/R630, R687/R630 and R690/R630 were sensitive to Fv/Fm measured in leaves. Such indices which are sensitive to changes in the curvature in the red reflectance region as a response to the effects of both PSI and PSII fluorescence emission on leaf reflectance also showed a correlation with diurnal changes in Fv/Fm (Zarco-Tejada et al., 2000a,b). At the canopy level in the laboratory and under natural light conditions, red edge indices were assessed for detection of chlorophyll fluorescence, including red edge spectral derivative indices D730/D706, DP21 (Dλp/D703), where λp is the inflection point of the reflectance spectrum in the red edge spectral region, and the curvature index R683^2/(R675·R691), which are both also related with chlorophyll $a+b$ (Cab) content. In subsequent studies Zarco-Tejada et al. (2000b, 2003) suggested that a *double-peak* feature in the 690–710 nm spectral region seen in the derivative reflectance was possibly due to the combined effects of fluorescence emission and low Cab content on stressed vegetation, implying potentially important applications in vegetation stress detection using passive hyperspectral remote sensing methods. Reflectance difference measures and derivative indices D705/D722, DP22 (Dλp/D720), and DPR1 (Dλp/Dλp + 12), were associated with water and heat stress conditions, observed during the recovery after the diurnal experiment (Zarco-Tejada et al., 2003). DPi, calculated as (D688·D710)/D697^2, and the area of the *double-peak* feature, Adp, were shown to track steady-state fluorescence Fs variation during both short and long-term stress induction stages in these canopy-level laboratory experiments.

Recent studies have demonstrated the fluorescence *in-filling* of the O_2-A atmospheric oxygen absorption band at 760 nm, as a detectable radiance signal at the near-canopy levels (Evain et al., 2004; Liu et al., 2005; Moya et al., 2004; Pérez-Priego et al., 2005). At the airborne and far-field scales, Maier et al. (2002) and Zarco-Tejada et al. (2004) reported the potential detection of the solar-induced fluorescence signal on apparent reflectance obtained from airborne sensors *Reflective Optics System Imaging Spectrometer* (ROSIS) and *Compact Airborne Spectrographic Imager* (CASI) based on the *in-filling* of fluorescence in the 760 nm atmospheric oxygen absorption band. However, no field validations were available in these studies to fully support the hypothesis presented.

On the modeling side, chlorophyll fluorescence effects on apparent reflectance at the leaf level were simulated with the *Fluorescence–Reflectance–Transmittance* (FRT) model (Zarco-Tejada et al., 2000a) and with the *Stochastic model for Leaf Optical Properties* (Maier et al., 1999; Maier, 2000). However, it was recognized that for simulation of chlorophyll fluorescence effects on apparent reflectance at the canopy level one needed to account for canopy scattering, within-canopy light level changes and viewing geometry effects. In response to this need, an integrated leaf-canopy model, the *Vegetation Fluorescence Canopy Model* (FluorMOD), was developed through a project funded by the European Space Agency (ESA) (http://www.ias.csic.es/fluormod). The FluorMOD project (Miller et al., 2004) coordinated the development of a leaf model FluorMODleaf (Pedrós et al., 2004, 2008) to simulate leaf fluorescence and a linked leaf-canopy model FluorSAIL (Verhoef, 2005) to simulate canopy fluorescence and scattered radiance, which were linked through an integrated interface FluorMODgui (Zarco-Tejada et al., 2006). This linked leaf-canopy FluorMOD model can be used to simulate diurnal effects of natural fluorescence on apparent canopy reflectance under varying viewing geometries, atmospheric characteristics and illumination dependence. Although the model requires further validation and refinement, currently FluorMOD can be used as a tool for understanding trends in leaf and canopy effects on fluorescence emission as function of viewing geometry and leaf and canopy inputs.

To make progress on the current status of our understanding of the potential for detection of solar-induced fluorescence signals in the presence of vegetation reflectance signatures, new research efforts requiring high spatial resolution imagery acquired at high spectral resolution are needed to validate fluorescence-sensitive red edge indices and *in-filling* signals for canopy chlorophyll fluorescence detection. The most definitive assessment of the viability of methods to retrieve the weak fluorescence signal can be made with high-resolution imagery targeting pure vegetation crowns without canopy architecture/closure effects, which it turns out are consistent with the assumptions made in developing the FluorMOD model. In addition, if frequent imagery acquisition is available to capture diurnal changes in water stress through short-term studies, as suggested in Berni et al. (2009) who used *unmanned aerial vehicle* (UAV) platforms for operational remote sensing in agricultural applications, then experimental research can examine above-canopy fluorescence detection methods as a function of changing stress status. This manuscript describes the results of such research aimed at making such progress through both simulation studies and airborne measurements. The FluorMOD reflectance–fluorescence model was used to provide an assessment of the suitability and sensitivity of fluorescence reflectance indices, as well as the *in-filling method*. This was complimented by data from airborne and field research to provide an assessment of the feasibility of detecting and imaging fluorescence using 1 nm FWHM bands at 757.5 and 760.5 nm with 15 cm spatial resolution, with a comparison to temperature changes detected with a thermal imager of 40 cm resolution onboard an UAV platform.

2. Materials and methods

2.1. Assessing the sensitivity of fluorescence indices and the in-filling method using the FluorMOD simulation model

2.1.1. Chlorophyll fluorescence detection with the in-filling method

The method to detect fluorescence emission based on the *in-filling* method was reported by McFarlane et al. (1980) in measurements of solar-induced natural fluorescence in vegetation canopies using the Fraunhofer H-α line at 656 nm, and Carter et al. (1990, 1996a, 2004) using H-α and the O_2-B atmospheric bands in leaf measurements. They also investigated the relationship between fluorescence and vegetation temperature at the image level as an indicator of plant stress (Carter et al., 1996b). More recent studies provided evidence

for fluorescence *in-filling* of the O_2-A atmospheric oxygen absorption band at 760 nm, as a detectable feature in the radiance spectra at the near-canopy levels (Evain et al., 2004; Liu et al., 2005; Moya et al., 2004; Pérez-Priego et al., 2005). The *in-filling* method uses the canopy radiance from *fluorescing* (vegetation) and *non-fluorescing* (soil) targets *in* and *out* of the oxygen line at 760.5 nm, defined as L_i^v, L_i^n, L_o^v, L_o^n respectively, to calculate reflectance R and fluorescence F [Eqs.(1) and (2)].

$$R = \frac{L_o^v - L_i^v}{L_o^n - L_i^n} \qquad (1)$$

$$F = L_i^v - R \cdot L_i^n \qquad (2)$$

This method was successfully used by Meroni et al. (2008a) at the leaf level, and at a canopy level by Moya et al. (2004) and Meroni et al. (2008b), showing that fluorescence emission can be detected using the O_2-A band at the leaf level and on a corn canopy under diuron herbicide penetration. Also, experiments conducted with narrow-band spectrometers (0.065 nm FWHM) (Pérez-Priego et al., 2005) showed that the observed canopy-level fluorescence *in-filling* with the O_2-A band at 760.5 nm was able to track the water stress status in orchard trees, demonstrating a link between *steady-state* chlorophyll

Table 1
FluorMOD model inputs used in this study to assess the sensitivity of reflectance indices using atmospheric, leaf and canopy inputs.

Atmospheric parameters			
Atmospheric file			FLUORMOD30V23.MEP
Irradiance			PAR dependence parameters: PARb = 0.0035; PARre = 0.005
Visibility			23 km
Solar zenith angle			30°
Viewing zenith angle			0°
Relative azimuth angle			0°
Leaf inputs			
N	1.8	Fi	0.06
Cab	30 μg/cm²	T	10 °C
Cw	0.025 cm	S	Broad bean
Cm	0.01 g/cm²	Sto	1.5
Canopy inputs			
Leaf area index		4	
LIDF parameter a		−0.5	
LIDF parameter b		−0.5	
Hot spot parameter		0.1	
Soil spectrum			
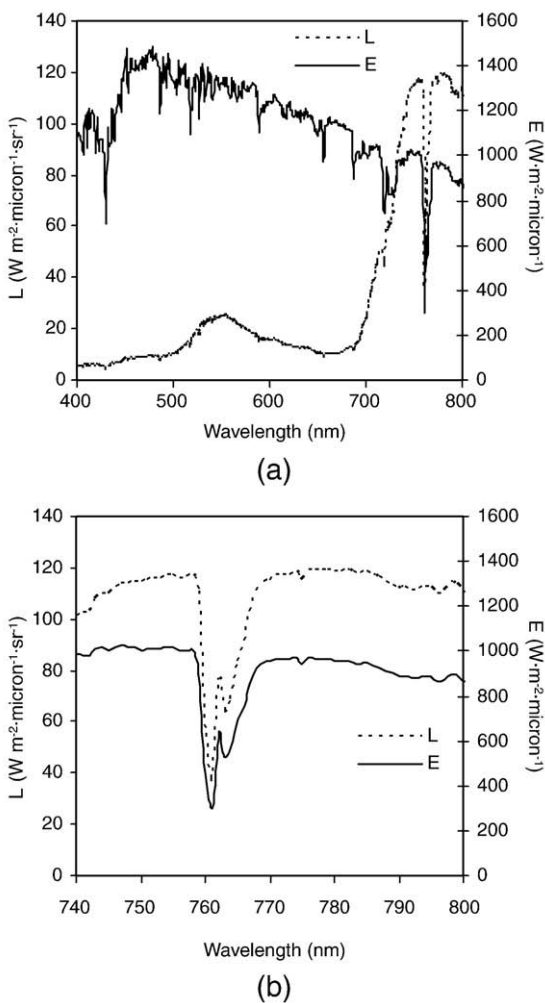
Fig. 1. FluorMOD model simulation of irradiance (E) and canopy radiance (L) at 1 nm resolution in the 400–800 nm range (a) and 740–800 nm (b), reproducing the fluorescence *in-filling* at O_2-A and O_2-B bands using atmospheric, leaf and canopy inputs from Table 1.

fluorescence (Fs, Ft) and *in-filling* of the 760 nm apparent reflectance of individual trees.

At the airborne scale, Maier et al. (2002) proposed an approach based on the *in-filling* method for the detection of the solar-induced fluorescence signal on apparent reflectance obtained from the airborne sensor *Reflective Optics System Imaging Spectrometer* (ROSIS) to estimate the *in-filling* of the 760 nm atmospheric oxygen absorption band by fluorescence emission. The method for *far-field* fluorescence detection through *in-filling* at the 690 and 762 nm oxygen bands requires the variables for the radiation flow (Maier et al., 2002; Zarco-Tejada et al., 2004). This method includes the influence of atmospheric transmittance between the target and the sensor along the view direction (T_v), the path radiance (L^{path}), and the global irradiance (E_G) at the scene target. The radiance *in* and *outside* the 762 oxygen absorption feature for non-fluorescing targets (L_o^n, L_i^n) are defined as,

$$L_o^n = \left(\frac{R_n E_{Go}}{\pi}\right) T_{Vo} + L_o^{path} \qquad (3)$$

$$L_i^n = \left(\frac{R_n E_{Gi}}{\pi}\right) T_{Vi} + L_i^{path} \qquad (4)$$

with the relationship between L_i^n and L_o^n as,
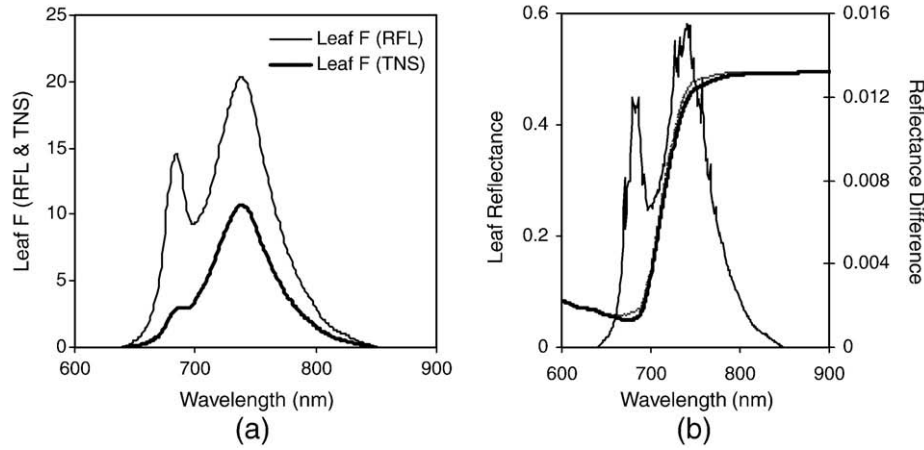
$$L_i^n = k_1 \cdot L_o^n + k_2 \qquad (5)$$

where,

$$k_1 = \frac{T_{Vi}\, E_{Gi}}{T_{Vo}\, E_{Go}}; k_2 = L_i^{path} - k_1 \cdot L_o^{path} \qquad (6)$$

In the case of fluorescing targets, such as vegetation, the radiance *in* and *outside* the oxygen absorption band are,

$$L_o^v = \left(\frac{R_v E_{Go}}{\pi} + L_f\right) \cdot T_{Vo} + L_o^{path} \qquad (7)$$

$$L_i^v = \left(\frac{R_v E_{Gi}}{\pi} + L_f\right) \cdot T_{Vi} + L_i^{path} \qquad (8)$$

Fig. 2. (a) FluorMOD leaf fluorescence, both reflected (RFL) and transmitted (TNS), for a simulated leaf with Fi = 0.049 and Cab = 43 µg/cm^2; (b) leaf reflectance with added simulated fluorescence (thin line) and without fluorescence (thick line), showing the reflectance difference.

with the relationship between L_i^V and L_o^V as,

$$L_i^V - k_3 \cdot L_f = k_1 \cdot L_o^V + k_2 \qquad (9)$$

where k_1 and k_2 are as in Eq. (6) and ,

$$k_3 = T_{Vi} - k_1 \cdot T_{vo} \qquad (10)$$

Therefore, coefficients k_1 and k_2 can be calculated from Eq. (5) using a set of non-fluorescing targets, enabling the calculation of fluorescence L_f from Eq. (9) for fluorescing targets, such as vegetation.

2.1.2. Fluorescence retrieval assessment using FluorMOD simulation

Through the FluorMOD project (Miller et al., 2004) a linked leaf-canopy model was developed that simulates chlorophyll fluorescence emission. The leaf model, FluorMODleaf (Pedrós et al., 2004) is linked to a canopy model, FluorSAIL (Verhoef, 2005), incorporating an excitation–fluorescence matrix, computed externally by means of the
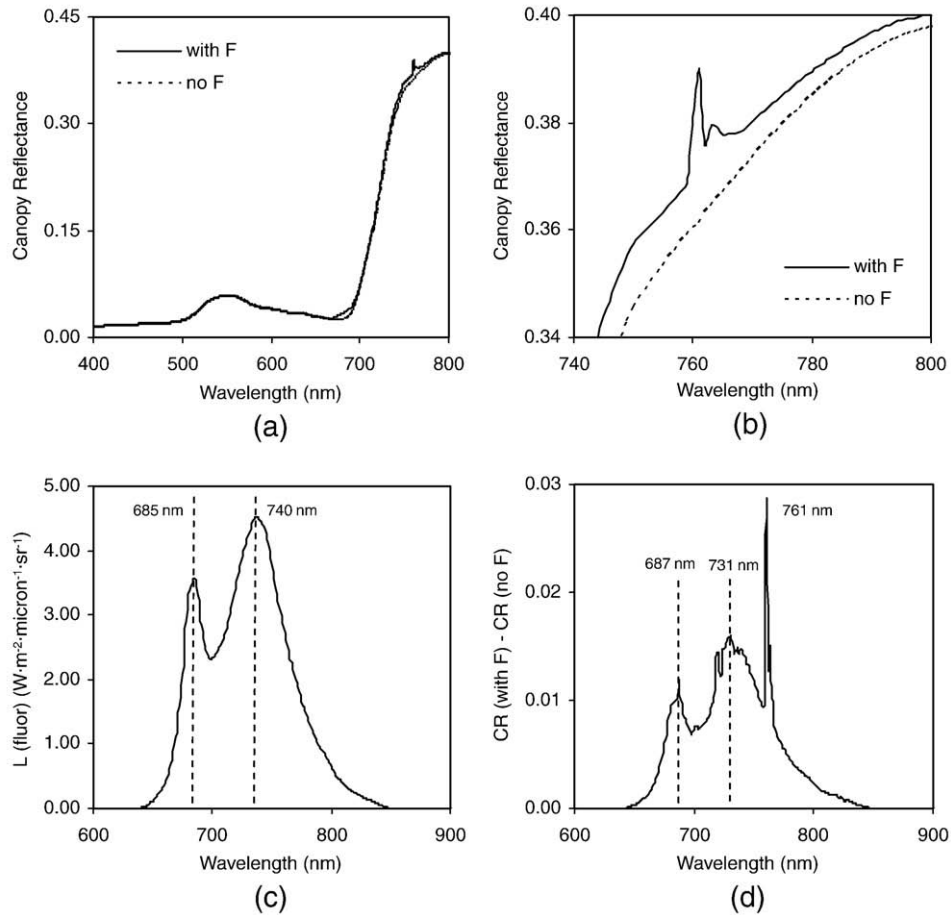
Fig. 3. Simulated canopy reflectance in the 400–800 nm range (a) and 740–800 nm (b) with (with F) and without (no F) fluorescence effects (inputs from Table 1). Fluorescence radiance (W·m^{-2}·micron^{-1}·sr^{-1}) (c) added to the canopy reflectance is extracted by reflectance difference calculation (d).
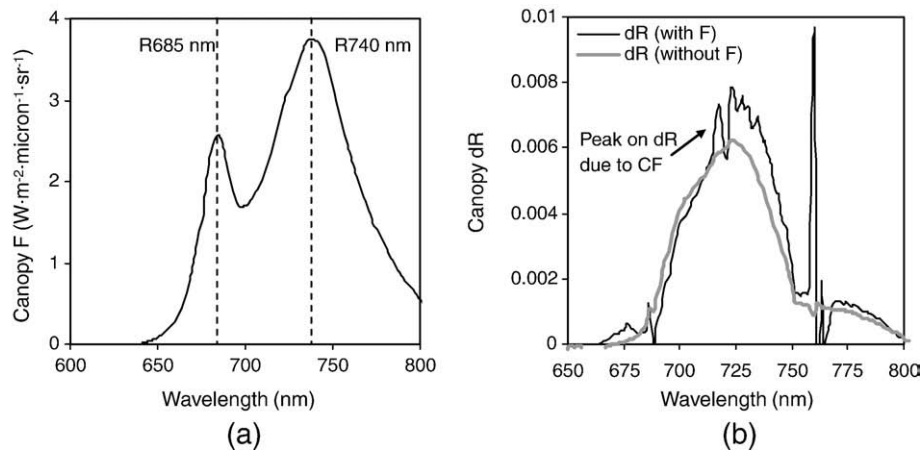
Fig. 4. Simulated fluorescence radiance corresponding to Fi = 0.049, Cab = 43 µg/cm² and LAI = 3.6 (other inputs from Table 1) (a) used to simulate the derivative canopy reflectance with and without fluorescence effects (b), showing a *double-peak* feature previously observed experimentally in Zarco-Tejada et al. (2003).

leaf-level fluorescence model, to simulate the fluorescence effects on the canopy signature (detailed information on the linked leaf-canopy models can be found in Zarco-Tejada et al. (2006)).

The inputs to the leaf model are the number of layers in PROSPECT (N); chlorophyll $a + b$ content in µg/cm² (C_{ab}); water equivalent thickness in cm (C_w); dry matter content in µg (C_m); fluorescence quantum efficiency (Fi); leaf temperature in degrees Celsius (T); species temperature dependence (S) (after Agati, 1998); and stoichiometry of PSII to PSI reaction centers (Sto), which depends on species and light conditions during plant growth. The canopy model requires the viewing zenith angle in degrees (Vza), relative azimuth angle in degrees (Raz), the canopy leaf area index (LAI), the hot spot parameter (h), and the leaf inclination distribution function (LIDF) parameters, LIDF$_a$ and LIDF$_b$. In addition, the canopy model requires a soil spectrum, and four outputs from the leaf model: leaf reflectance without fluorescence (RN), leaf transmittance without fluorescence (TN), and the upward (FuN) and downward (FdN) fluorescence matrices.

The FluorMOD model was used in this study to assess the sensitivity of reflectance indices described earlier, as a function of fluorescence emission, leaf chlorophyll concentration, and canopy leaf area index. The model simulates irradiance (E) and canopy radiance (L) at 1 nm resolution (Fig. 1), reproducing the fluorescence *in-filling* at O$_2$-A and O$_2$-B bands using atmospheric, leaf and canopy inputs (Table 1). The simulated leaf fluorescence, both reflected and transmitted (Fig. 2a), provides the expected effects at leaf level in the 650–850 nm spectral region (Zarco-Tejada et al., 2000a, 2003) as extracted by the reflectance difference method (Fig. 2b). The simulated irradiance and canopy radiance with and without fluorescence effects (inputs from Table 1) enables the assessment of the fluorescence peak experimentally observed in canopy reflectance (Fig. 3a and b). Canopy-level fluorescence effects are observed along the red edge region and particularly as an *in-filling peak* centered at 760.5 nm (Fig. 3b) when compared with the canopy reflectance without fluorescence effects. The fluorescence radiance (Fig. 3c superimposed on the apparent canopy reflectance can be extracted by a reflectance difference calculation (Fig. 3d), showing larger effects due to fluorescence emission at the 760 nm oxygen band (ca. 3% in this simulation example) as compared with the fluorescence emission for the rest of the spectral region (ca. 1.8% at the 735 nm band).

The effects of chlorophyll fluorescence on derivative reflectance could also be assessed using FluorMOD for comparison with previous results obtained experimentally in the laboratory or under natural light conditions. The fluorescence radiance corresponding to $Fi = 0.049$, Cab = 43 µg/cm² and LAI = 3.6 (other inputs from Table 1) (Fig. 4a) was used to simulate the derivative canopy reflectance with and without

fluorescence effects (Fig. 4b). Results indicate that the *double-peak* feature previously observed experimentally (Zarco-Tejada et al., 2003) is reproduced in these simulations of the canopy derivative reflectance when fluorescence effects are included. For a more detailed simulation study, the FluorMOD model was used to assess the expected
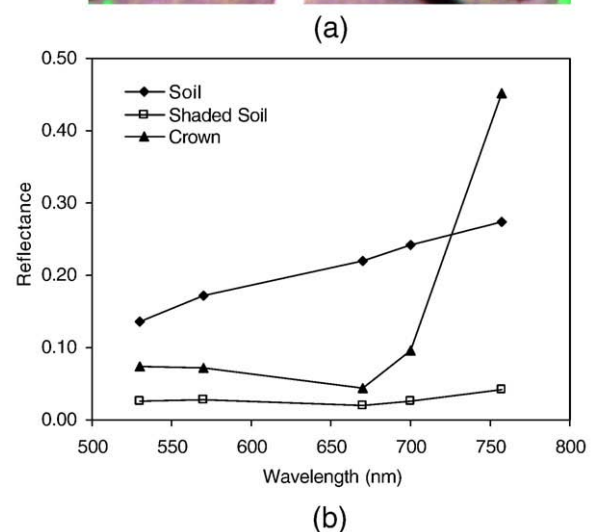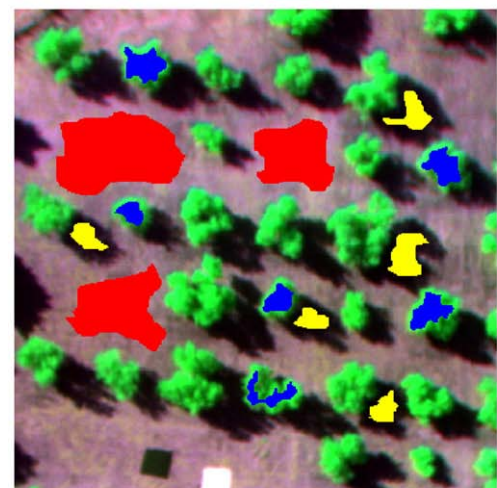
Fig. 5. Calibrated multispectral reflectance acquired at 10 nm FWHM and 15 cm spatial resolution (a), targeting crown, shaded and sunlit soil spectra (b).

fluorescence effects and fluorescence retrieval capability as function of input parameters F_i, Cab and LAI on: i) the fluorescence *in-filling* method; ii) reflectance indices; and iii) derivative indices; results are reported in Section 3.1.

## 2.2. Field experiments and airborne campaigns

An airborne multispectral camera with two 1 nm FWHM filters in the 757.5 and 760.5 nm bands, and four 10 nm FWHM bands in the 400–800 nm spectral region was flown over 4 study sites, at 15 cm spatial resolution. Three orchards (peach, orange and olive groves) were used for deficit irrigation experiments to produce a gradient in water stress levels. In addition, a variety trial olive orchard was selected to provide a gradient in chlorophyll concentration and photosynthesis as function of genetic variety conditions.

2.2.1. Field data collection

Study sites were located in southern Spain, consisting of *Olea europaea* L. cv. 'Arbequino' (olive), *Prunus persica* L. Batsch cv. 'Baby Gold 8' (peach) and *Citrus sinensis* L. cv. 'Lanelate' (orange) groves planted in regular patterns under drip irrigation. One of the *O. europaea* L. study sites consisted of a rain-fed variety test field, representing a very heterogeneous grove because of the large number of varieties planted in comparison to a typical commercial olive orchard. The climate of the area is Mediterranean with an average annual rainfall of 650 mm, concentrated from autumn to spring, and a reference evapotranspiration (ET) of 1390 mm.

The olive, peach and orange orchards belong to a network of study sites irrigated under regulated deficit irrigation (RDI) (Fereres & Soriano, 2007). The olive orchard was irrigated with three drip treatments randomly applied within an area of 6 rows of 18 olive trees (2646 m^2): i) irrigated at 3.2 mm/day (well irrigated treatment, C); ii) 0.8 mm/day (deficit treatment, S1); and iii) an intermittent treatment, with 1.3 mm/day from 7 May to 15 July and from 24 September to 7 October, stopping irrigation from 15 July to 24 September (deficit treatment, S2). The peach orchard had part of the field under regulated deficit irrigation while the other part had an ample water supply. The RDI part of the orchard received no irrigation until the period of rapid expansion of fruit growth (Phase III), irrigation over full ET for one week and then with constant doses at full ET until harvest. The orange orchard was divided into plots under RDI and full ET irrigation, where the RDI plot received 65% of the water relative to the full ET part of the field.

A Scholander pressure bomb (PWSC Model 3000, Soilmoisture equipment Corp., California, USA) was used to measure leaf water potential weekly on selected trees in each orchard at noon. Stomatal conductance was measured weekly with a leaf steady-state porometer (model PMR-4, PP Systems, Hitchin Herts, Great Britain). Leaf chlorophyll fluorescence measurements were conducted under field conditions using the *Pulse-Amplitude-Modulated Fluorometer* PAM-2100 (Heinz Walz GMBH, Effeltrich, Germany), measuring at the time of flight acquisitions steady-state F_s fluorescence on 30 leaves per tree on 8 trees (olive orchard), 10 trees (peach orchard), 8 trees (orange orchard), and 13 trees (olive variety field), respectively. Leaf
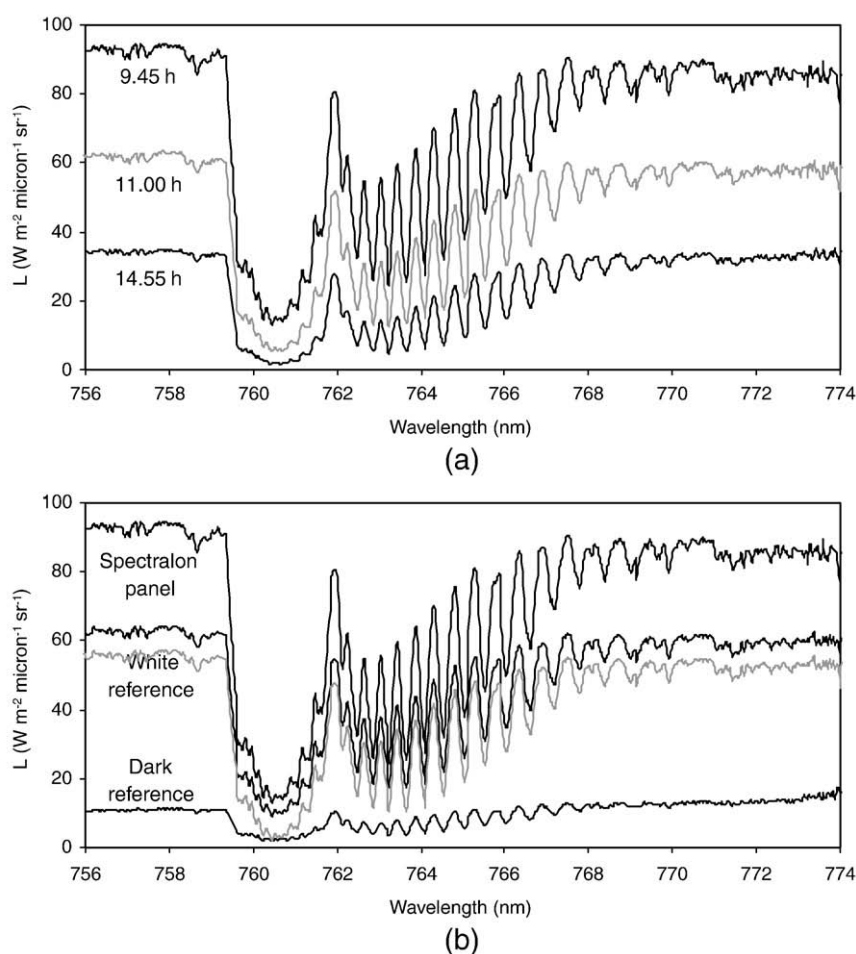
Fig. 6. Diurnal measurements of the white spectralon reference panel radiance conducted at the time of flight acquisitions (a) at 0.065 nm spectral resolution in the O$_2$-A spectral region (756–774 nm). White and dark target radiance used for airborne image calibration at 760.5 and 757.5 nm bands (b).

photosynthesis, stomatal conductance and fluorescence were measured using the *Portable Gas Exchange Fluorescence System* GFS-3000 (Heinz Walz GMBH, Effeltrich, Germany) on 2 leaves per tree on 10 trees of the olive variety trial orchard at the time of airborne image acquisition.

2.2.2. Airborne campaigns

An *unmanned aerial vehicle* (UAV) platform was developed to carry a payload with thermal and multispectral imaging sensors for remote sensing operations (Berni et al., 2009). The multispectral sensor used in this study was a 6-band multispectral camera (MCA-6, Tetracam, Inc., California, USA). The camera consists of 6 independent image sensors and optics with user-configurable spectral filters. The image resolution is 1280×1024 pixels with 10-bit radiometric resolution and optics focal length of 8.5 mm, yielding an angular FOV of $42.8° \times 34.7°$ and 15 cm pixel spatial resolution at 150 m flight altitude. The detector used is a CMOS sensor with pixel size 5.2 µm × 5.2 µm, image area 6.66 mm × 5.32 mm, operated in a progressive scan mode, at 54 dB signal-to-noise ratio, with <0.03% fixed pattern noise, 28 mV/s dark current, and 60 dB dynamic range. Multispectral images acquired over each study site enabled tree identification for field validation purposes on the olive, peach, orange and olive variety trial fields. Different bandsets were selected depending on the objectives adopted for the remote sensing study, including 25 mm diameter bandpass filters of 10 nm FWHM (Andover Corporation, NH, USA), with center wavelengths at 490 nm, 530 nm, 550 nm, 570 nm, 670 nm, 700 nm, 750 nm, and 800 nm, and two 1 nm FWHM filters centered at 760.5 and 757.5 nm bands for fluorescence *in-filling* measurements. Filter transmission measurements were conducted with a Li-Cor 1800-12 Integrating Sphere (Li-Cor, Inc., Lincoln, NE, USA), coupled by a 200 µm diameter single mode fiber to an Ocean Optics model HR2000 spectrometer (Ocean Optics Inc., Dunedin, FL, USA), with a 2048 element detector array, 0.05 nm sampling interval and 0.065 nm spectral resolution in the 678.76–774.05 nm range. Measurements of the 1 nm filters yielded transmissions of 49.2% and 46.8%, and bandpasses FWHM = 1.57 nm (center wavelength 760.47 nm), and FWHM = 1.6 nm (center wavelength 757.42 nm), respectively. For the 10 nm filters measurements yielded ca. 60% transmission and 10.4 nm FWHM.

Study sites were also imaged with the airborne platform using a thermal camera to derive surface temperature of each tree under study. The thermal imager used was the Thermovision A40M (FLIR, USA) equipped with a 40° FOV lens and connected to computer via IEEE-1394 protocol. The image sensor is a Focal Plane Array (FPA) based on uncooled microbolometers with a resolution of 320×240 pixels and spectral response in the range 7.5–13 µm, yielding 38 µm × 38 µm pixel size in the 7.5–13 µm region, with 0.08 K sensitivity at 303 K. The camera delivers digital raw images at 16 bits of *at-sensor* calibrated radiance with a dynamic range of 233 K–393 K. The sensor implements an internal calibration for *non-uniformity correction* (NUC) and internal temperature calibration. Thermal images from each study site were acquired at 40 cm pixel resolution enabling the retrieval of pure crown average temperature from each tree under study.

Image atmospheric correction and calibration methods were conducted to generate spectral reflectance and surface temperature, respectively. Multispectral image calibration was conducted using the empirical line method (Smith & Milton, 1999) by placing two 2×2 m levelled dark and white targets in a central location within the flight path of the UAV platform. Field spectral measurements were taken on the calibration targets with an ASD Field Spectrometer (FieldSpec Handheld Pro, ASD Inc., CO, USA) in the 350–1050 nm spectral range at the time of image acquisition. The ASD Field Spectrometer was first calibrated using a Spectralon (SRT-99-180, LabSphere, NH, USA) white panel, therefore enabling the calculation of white and dark panel reflectance spectra to be used later for the empirical line calibration method. Calibrated multispectral reflectance imagery at 10 nm FWHM was obtained (Fig. 5a), while targeting pure components such as

crown, shaded and sunlit soil spectra (Fig. 5b). Field validation campaigns for reflectance retrieval yielded an RMSE = 1.17% ($n = 90$) after empirical line methods were applied at each flight time (Berni et al., 2009).

The 1 nm FWHM multispectral camera bands centered at 760.5 and 757.5 nm later used for the fluorescence *in-filling* retrieval method were calibrated using the Ocean Optics model HR2000 spectrometer
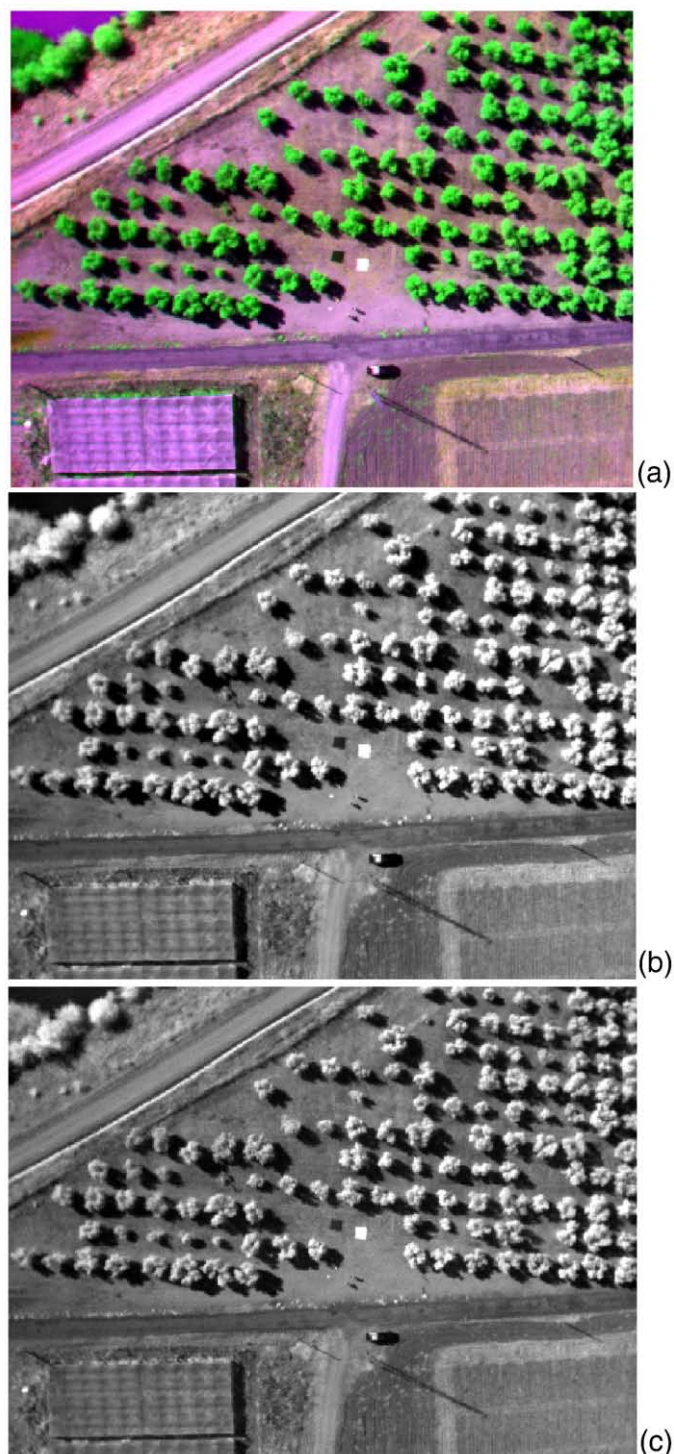

Fig. 7. Calibrated images at 10 nm FWHM (a), and 1 nm FWHM at 757.5 nm (b) and 760.5 nm (c) used to extract crown radiance (fluorescing) and soil radiance (non-fluorescing) targets to estimate crown chlorophyll fluorescence using the *in-filling* method.
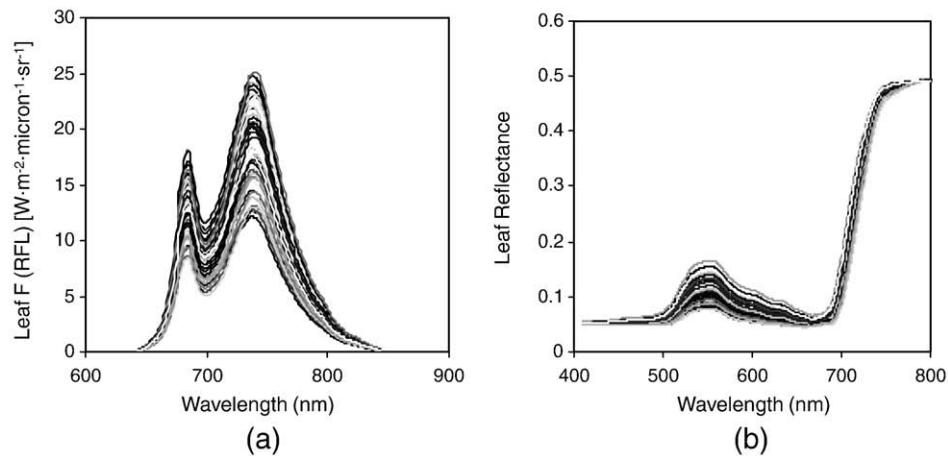
Fig. 8. Synthetic leaf spectra generated with FluorMOD using random input parameters Fi (0.03–0.06), Cab (30–80 µg/cm^2), and LAI (2–4). Leaf fluorescence emission [W·m^{-2}·micron^{-1}·sr^{-1}] (a) and leaf reflectance (b) show a wide range of both fluorescence and chlorophyll content variation.

(Ocean Optics Inc., Dunedin, FL, USA) at 0.065 nm spectral resolution in the 678.76–774.05 nm spectral range. The HR2000 instrument was calibrated to irradiance (E_g) in the laboratory with a cosine corrector-diffuser illuminated by the LS-1-CAL calibrated tungsten halogen NIST-traceable light source (Ocean Optics, Dunedin, FL, USA), and calibrated to radiance (L) with the Spectralon panel (Labsphere, North Sutton, USA). Diurnal measurements of the Spectralon (SRT-99-180, LabSphere, NH, USA) white panel radiance were conducted in the field

at the time of flight acquisitions (Fig. 6a) at 0.065 nm spectral resolution in the O$_2$-A spectral region (756–774 nm), yielding white and dark target radiance used for airborne image calibration at 760.5 and 757.5 nm bands (Fig. 6b). Calibrated images at 10 nm FWHM (Fig. 7a), and 1 nm bandwidth at 757.5 nm (Fig. 7b) and 760.5 nm (Fig. 7c) were used to extract radiances from tree crown (fluorescing) and soil (non-fluorescing) targets used to estimate crown chlorophyll fluorescence using the *in-filling* method.
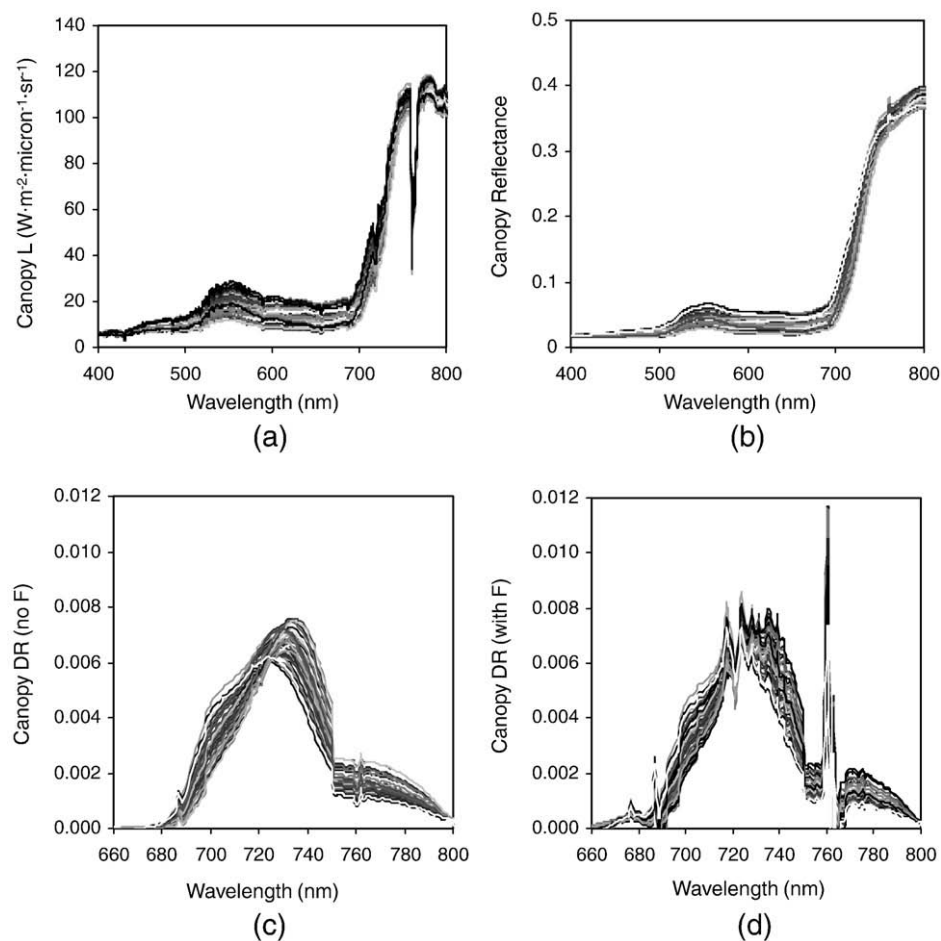
Fig. 9. Simulations conducted with FluorMOD model for parameters Fi (0.03–0.06), Cab (30–80 µg/cm^2), and LAI (2–4) for canopy radiance (a) and canopy reflectance (b). Simulated canopy derivative reflectance without fluorescence (c) and with fluorescence (d) show a peak at 721 nm due to fluorescence effects, a *double-peak* feature previously observed experimentally in Zarco-Tejada et al. (2003).

Table 2
Relationships (determination coefficients calculated as the square of the Pearson product-moment correlation coefficient) obtained between FluorMOD inputs and fluorescence estimates using the *in-filling* method (*F*), reflectance and derivative reflectance indices sensitive to chlorophyll fluorescence.

|	*Fi*	*Cab*	*LAI*	*Fi·Cab·LAI*	*Fi·LAI*	*Fi·Cab*	*Cab·LAI*	$L(F)_{761}$
In-filling method								
F	0.69	**0.33**	**0.05**	0.83	0.56	0.81	0.37	**0.82**
Derivative indices								
D702/D680	0.78	**0.27**	**0.039**	0.46	0.24	0.79	0.07	**0.78**
D705/D722	0	0.85	0.049	0.41	0	0.38	0.74	0
D730/D706	0	0.92	0.05	0.56	0.04	0.54	0.8	0.04
D735/D680	0.24	0.44	0.12	0.11	0.01	0.03	0.59	0.13
D761/D757	0.58	0.19	0.09	0	0.09	0	0.29	0.41
DPi (D688·D710)/D697^2	0.19	0.73	0	0.59	0.08	0.86	0.41	0.26
Reflectance indices								
R761−R757	0.72	**0.26**	**0.08**	0.82	0.64	0.74	0.34	**0.85**
R750/R710	0	0.54	0.37	0.66	0.21	0.3	0.98	0.04
R690/R630	0.56	**0.34**	**0.07**	0.89	0.57	0.75	0.44	**0.71**
R735/R850	0	0.78	0.16	0.59	0.08	0.41	0.92	0.02
R761/R757	0.65	**0.4**	**0.03**	0.84	0.49	0.86	0.39	**0.78**
R740/R685	0.03	0	0.97	0.15	0.35	0.02	0.34	0
R740/R850	0	0	0.99	0.21	0.49	0	0.35	0.01
R685/R850	0.02	0.02	0.89	0.25	0.34	0	0.5	0
R740/R630	0	0.03	0.92	0.4	0.5	0.01	0.59	0.03
R680/R630	0.27	0.75	0	0.66	0.1	0.87	0.44	0.35
R685/R630	0.35	0.67	0	0.76	0.2	0.89	0.47	0.46
CUR R683^2/(R675·R691)	0.27	0.74	0	0.79	0.2	0.85	0.59	0.37

The synthetic random spectra were generated varying fluorescence efficiency (*Fi*), leaf chlorophyll concentration (*Cab*) and canopy leaf area index (*LAI*). In bold are shown indices with high relationship with L(F)761 ($r^2 > 0.7$), and low relationships with both Cab and LAI ($r^2 < 0.4$).

Surface temperature was obtained applying atmospheric correction methods to thermal imager data based on MODTRAN radiative transfer model. Local atmospheric conditions were determined by air temperature, relative humidity and barometric pressure measurements at the time of flight using a portable weather station (Model WXT510, Vaisala, Finland) and were used as input into the MODTRAN model. A single-
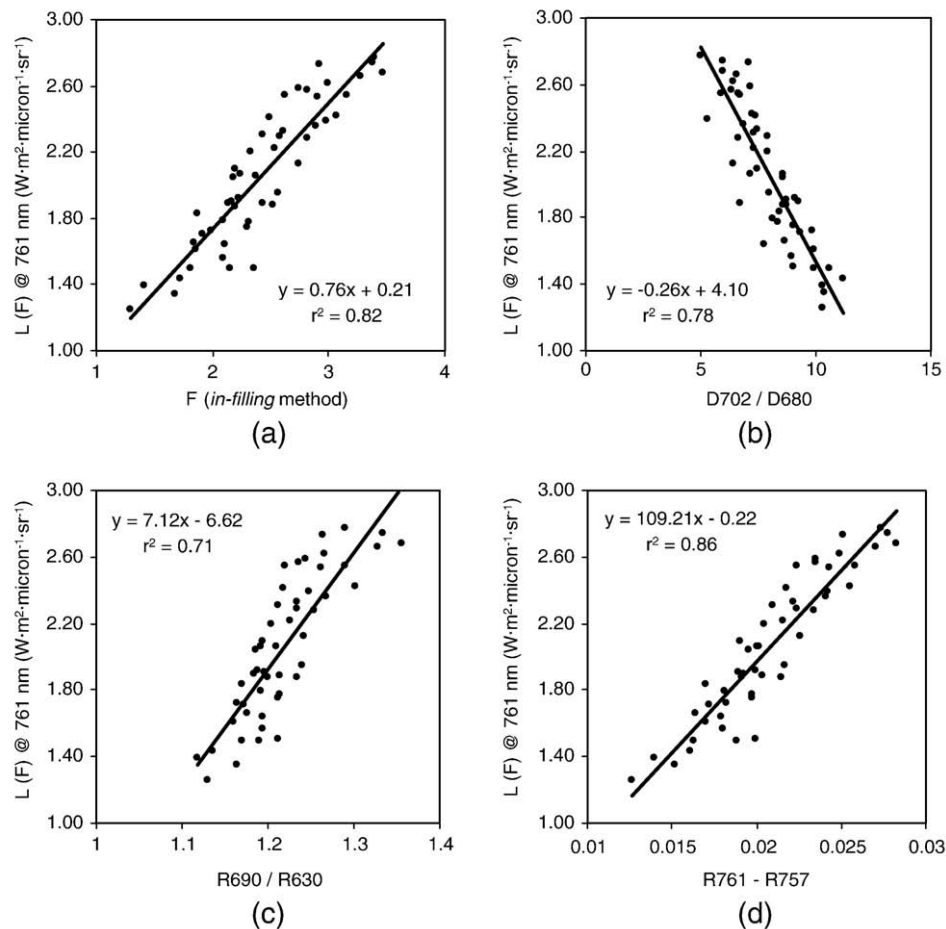
Fig. 10. Fluorescence retrievals from the synthetic canopy reflectance simulations using the *in-filling* method (*F*) (a), derivative index D702/D680 (b), and reflectance indices R690/R630 (c), and R761–R757 (d).

(a)

(b)
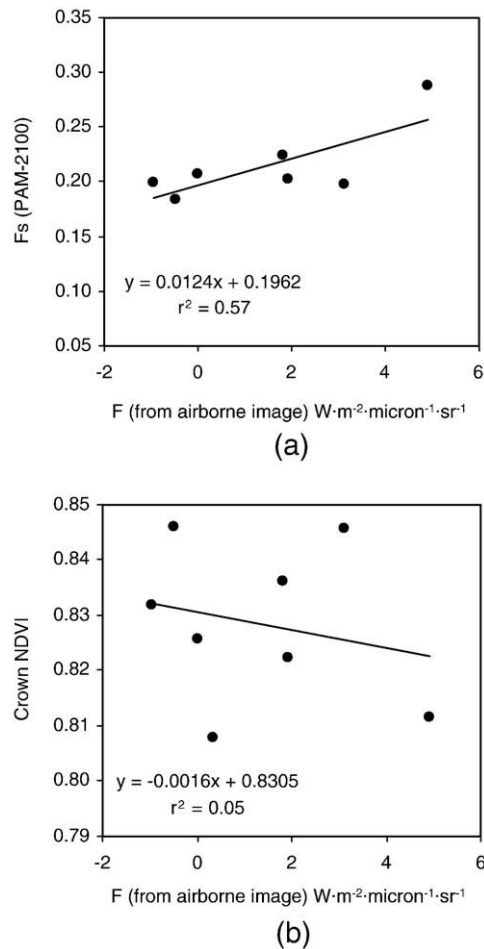
Fig. 11. Relationship obtained between ground-truth *Fs* (PAM-2100) and fluorescence extracted from the airborne image using the *in-filling* method in a water stress experiment conducted on an olive orchard (a); crown NDVI showed no relationship with crown fluorescence extracted from the imagery (b) to dismiss structural effects on the fluorescence retrieval.

layer atmosphere with uniform conditions was considered for the simulations since the variation for the typical UAV flight altitude (150–200 m) could be neglected. Atmospheric correction methods conducted showed the successful estimation of surface temperature images of 40 cm spatial resolution, yielding RMSE <1 K (Berni et al., 2009).

3. Results

3.1. Simulation results

The FluorMOD model was used to generate spectra using random input parameters Fi (0.03–0.06), Cab (30–80 μg/cm^2), and LAI (2–4). Leaf fluorescence emission (Fig. 8a) and leaf reflectance (Fig. 8b) show a wide range of responses to both fluorescence and chlorophyll content variation in the generated set of synthetic spectra. Fluorescence, chlorophyll and leaf area index effects could be observed on the synthetic canopy radiance generated (Fig. 9a) and on the simulated canopy reflectance (Fig. 9b). Canopy derivative reflectance calculations from the synthetic spectra simulated by FluorMOD for the spectra without (Fig. 9c) and with (Fig. 9d) fluorescence effects demonstrated the red edge peak shift toward longer wavelengths due to the variation of the chlorophyll content (Fig. 9c) and the *double-peak* feature observed on the derivative spectra when fluorescence effects are included (Fig. 9d).

This set of random synthetic spectra simulated by FluorMOD as function of fluorescence efficiency (Fi), leaf chlorophyll concentration

(Cab) and canopy leaf area index (LAI) for canopy radiance (Fig. 9a), canopy reflectance (Fig. 9b) and canopy derivative reflectance (Fig. 9d) were used to retrieve fluorescence (*F*) using the *in-filling* method, and to calculate reflectance and derivative reflectance indices sensitive to chlorophyll fluorescence (Table 2). The retrieved fluorescence using the *in-filling* method (*F*), and the reflectance and derivative reflectance indices were compared with the canopy radiance fluorescence ($L(F)_{761}$) simulated by FluorMOD. In addition, the fluorescence retrieval (*F*) and fluorescence-sensitive indices were compared with input parameters Fi, Cab and LAI, in order to assess the sensitivity of the retrieved fluorescence (*F*) and the calculated indices with leaf chlorophyll content and leaf area index (Table 2).

The fluorescence retrievals using the *in-filling* method (*F*) ($r^2 = 0.82$) (Fig. 10a), derivative index D702/D680 ($r^2 = 0.78$) (Fig. 10b) and reflectance indices R690/R630 ($r^2 = 0.71$) (Fig. 10c), R761–R757 ($r^2 = 0.86$) (Fig. 10d), and R761/R757 ($r^2 = 0.78$) yielded the best results in the simulation study. These indices were found to be insensitive to LAI variation (r^2 with LAI ranged from 0.03 to 0.08), with low Cab sensitivity for the fluorescence *in-filling* method ($r^2 = 0.33$ for Cab vs. F), D702/D680 ($r^2 = 0.27$ for Cab vs. the index), R761–R757 ($r^2 = 0.26$ for Cab vs. the index).

On the other hand, through this simulation study, other indices generally accepted for fluorescence detection at leaf and canopy levels were found to show high sensitivity to LAI and Cab variations; in particular, R740/R685, R740/R850, R685/R850, R740/R630 were highly affected by LAI (r^2 ranging between 0.89 and 0.97) with little sensitivity to fluorescence. Indices D705/D722, D730/D706, DPi, R735/R850, R680/R630, R685/R630, and the curvature index R683^2/(R675·R691) were highly affected by Cab (r^2 ranging between 0.67 and 0.92).

This simulation study demonstrates the retrieval capability of the *in-filling* method even when other common effects such as variations in chlorophyll content and leaf area index are considered. Moreover, it shows that some fluorescence-sensitive indices published in the literature are highly affected by chlorophyll and structural effects.

3.2. Experimental results

Fluorescence extracted per tree from the airborne imagery using the *in-filling* method with the 1 nm FWHM 757.5 and 760.5 nm bands was compared with field-measured chlorophyll fluorescence data on the four orchards. The water stress experiments conducted on olive and peach orchards demonstrated the feasibility of chlorophyll fluorescence extraction at the tree level from the airborne imagery, yielding determination coefficients $r^2 = 0.57$ (Fig. 11a, olive), and $r^2 = 0.52$ (Fig. 12, peach). In both cases fluorescence extracted from airborne imagery using the *in-filling* method was compared with
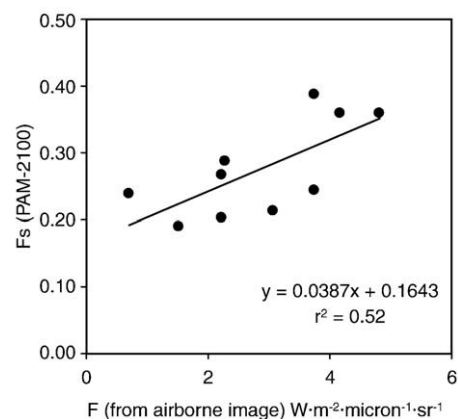
Fig. 12. Relationship obtained between ground-truth *Fs* (PAM-2100) and fluorescence extracted from the airborne image using the *in-filling* method in a water stress experiment conducted on a peach orchard.
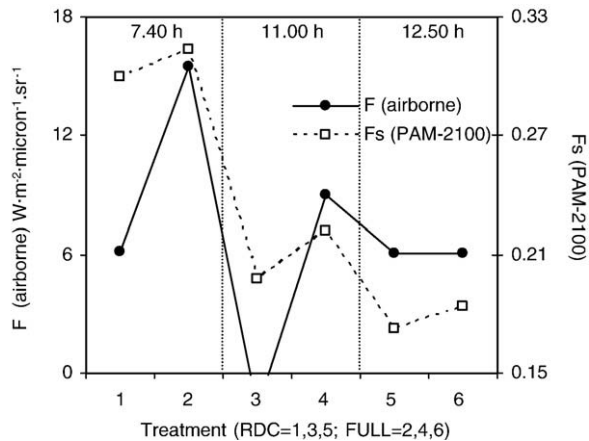
Fig. 13. Diurnal trend for both airborne fluorescence (F) and field measured fluorescence (Fs) using the PAM-2100 instrument acquired at 7.40, 11.00 and 12.50 GMT. Water stress trees (labelled as 1, 3, 5) yielded lower values than well-irrigated trees (labelled as 2, 4, 6).

field-measured steady-state fluorescence (Fs) using the PAM-2100 instrument. In order to address potential structural effects on fluorescence retrievals from the airborne imagery, such as the influence of tree LAI, crown NDVI was extracted and shown to exhibit no relationship with crown fluorescence extracted from the imagery ($r^2 = 0.05$; Fig. 11b; olive), demonstrating the sensitivity of R757.5 and R760.5 nm bands to fluorescence and the absence of crown LAI influences. The consistency of airborne fluorescence retrievals

from trees under water stress condition (higher F values on full irrigated than deficit-watered trees) was compared with the mean crown temperature estimated from the airborne imagery. The full irrigated peach trees yielded $F = 3.8$ W·m^{-2}·µm^{-1}·sr^{-1} and crown temperature $T = 309.2$ K, while deficit irrigation trees yielded $F = 2.2$ W·m^{-2}·µm^{-1}·sr^{-1} and crown temperature $T = 310.49$ K. Therefore, full-irrigated trees yielded higher F and lower T than deficit-irrigation trees, as expected under water stress conditions (Pérez-Priego et al., 2005; Sepulcre-Cantó et al., 2006). Negative values found in some of the fluorescence *in-filling* estimates when F is close to 0 (low fluorescence signals) were due to noise levels being similar to the low signals measured, as well as potential image registration displacements between the 757.5 and 760.5 nm bands.

The multispectral airborne images collected at 7.40, 11.00 and 12.50 GMT over the orange orchard showed a consistent trend for both airborne fluorescence F and field-measured fluorescence using the PAM-2100 instrument (Fig. 13). In all cases airborne-estimated F and PAM-2100 Fs from trees under stress (labelled as 1, 3, 5 in Fig. 13) yielded lower values than well-irrigated trees (labelled as 2, 4, 6 in Fig. 13) when collected at the same time. In addition, a decrease in chlorophyll fluorescence over the diurnal interval was consistent with the diurnal change experimentally observed in photosynthesis in the trees under stress, yielding $r^2 = 0.6$ (data not shown) between airborne F and assimilation (A) measured in the field with the GFS-3000 instrument. Similar results were obtained between airborne F and ground truth assimilation measured in the olive variety field experiment under no water stress levels, yielding $r^2 = 0.71$ (Fig. 14a), and $r^2 = 0.54$ between airborne F and Yield (Fig. 14b). Quenching parameters, qP and qN measured with PAM-2100 were related with
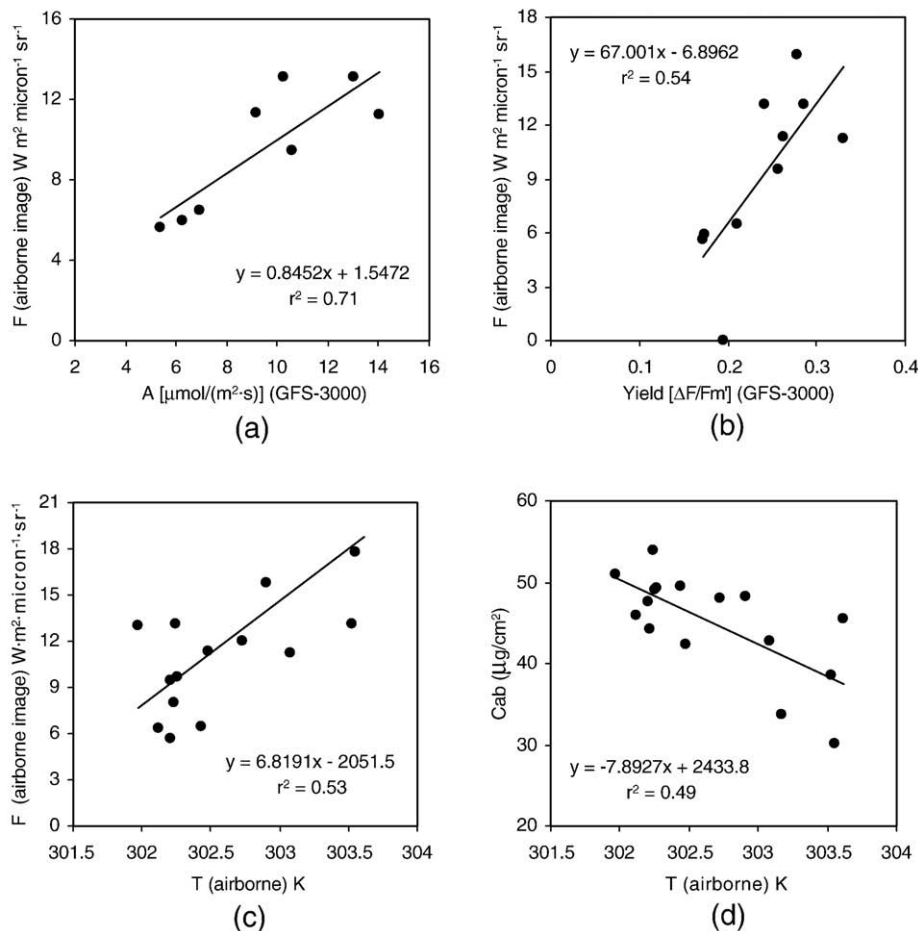
Fig. 14. Results obtained between airborne fluorescence estimates and ground truth assimilation (a) and yield (b) measured in the olive variety trial experiment. Relationships obtained between airborne crown temperature and airborne fluorescence (c) and airborne-estimated chlorophyll content (d).
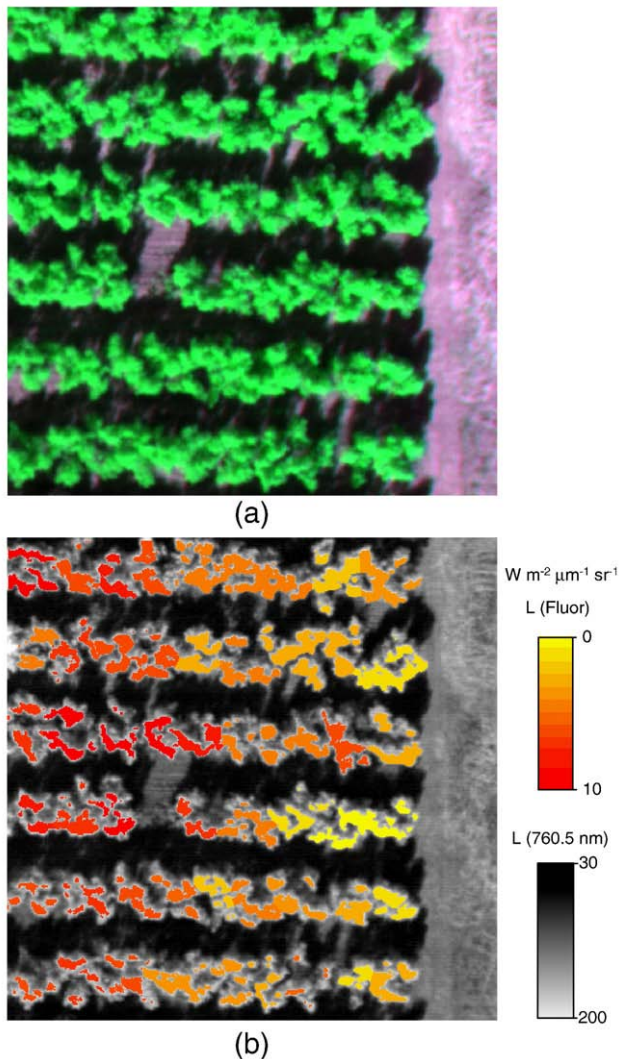
Fig. 15. Image of the fluorescence estimates acquired at 15 cm pixel resolution using the *in-filling* method at the crown level from the multispectral image (a), showing the spatial variability of the vegetation fluorescence *in-filling* within the orchard (b).

airborne *F*, yielding $r^2 = 0.29$ and $r^2 = 0.21$ respectively, suggesting a link with both photochemical and non-photochemical quenching. This link was further investigated assessing the relationships between airborne *F* and estimated chlorophyll content with crown *T*, yielding $r^2 = 0.53$ (Fig. 14c) and $r^2 = 0.49$ (Fig. 14d), respectively. These results demonstrate the physiological link between airborne estimated *F* and *T*, and it suggests a successful retrieval of fluorescence at the crown level using the fluorescence *in-filling* method. Results shown in Fig. 14 are all consistent, except for the direct relationship found between *F* and *T*. The hypothesis that could clarify this *F* vs. *T* relationship may be explained by the confounding effects caused on both *F* and *T* by the different varieties in the trial, which showed variability in Cab and LAI. An image of the fluorescence *in-filling* acquired at 15 cm pixel resolution from the multispectral image (Fig. 15a) using the *in-filling* method at the crown level was produced, showing the spatial variability of the vegetation fluorescence *in-filling* within the orchard (Fig. 15b).

4. Conclusions

The work reported in this manuscript demonstrates that imaging solar-induced chlorophyll fluorescence emission using the *in-filling* method is feasible. The multispectral camera used 1 nm FWHM bands located at 757.5 and 760.5 nm, at 15 cm pixel resolution while flown at

150 m above the crop canopies. Field experiments conducted in olive, peach, orange (water stress trials), and olive orchard (variety trial) generated fluorescence emission variability as function of the stress status. Chlorophyll fluorescence detection was conducted from the 1 nm FWHM radiance imagery at the crown level, targeting pure vegetation pixels to avoid background and shadow effects. Both spatial variability of fluorescence emission within the orchard as function irrigation supplies, as well as diurnal experiments demonstrated successful fluorescence retrieval capability and consistent estimates of fluorescence using the *in-filling* method applied to the airborne imagery.

Simulations with the FluorMOD model were used to assess fluorescence retrieval capability of both the *in-filling* method and published fluorescence–reflectance indices using a random set of synthetic spectra and variation of inputs including fluorescence efficiency, leaf chlorophyll content and canopy leaf area index. Canopy radiance, reflectance and derivative reflectance were used to assess the retrieval capability of fluorescence. The results of the simulation study proposed that fluorescence retrievals are best done using the *in-filling* method, the derivative index D702/D680 and reflectance indices R690/R630, R761–R757, and R761/R757. The above-mentioned indices were insensitive to LAI variation (r^2 with LAI ranging from 0.03 to 0.08), with low Cab sensitivity for the fluorescence *in-filling* method, D702/D680, and R761–R757. On the other hand, other published indices generally accepted for fluorescence detection at leaf and canopy levels were demonstrated in this simulation study to exhibit high sensitivity with Cab and LAI. In particular, R740/R685, R740/R850, R685/R850, R740/R630 were highly affected by LAI (r^2 ranging between 0.89 and 0.97) with little sensitivity to fluorescence. Indices D705/D722, D730/D706, DPi, R735/R850, R680/R630, R685/R630, and the curvature index $R683^2/(R675 \cdot R691)$ were highly affected by Cab. The simulation study demonstrated the retrieval capability of the *in-filling* method even when other common effects such as chlorophyll content and leaf area index effects are considered. Moreover, other fluorescence-sensitive indices published in the literature are highly affected by chlorophyll and structural effects, and care must be taken when using indices in field conditions that are potentially affected by such undesired leaf and canopy effects.

The FluorMOD fluorescence model enabled the simulation of the fluorescence effects on canopy derivative reflectance, assessing previous results obtained experimentally in the laboratory or under natural light conditions. Canopy derivative reflectance calculated from the synthetic spectra simulated without and with fluorescence effects demonstrated the red edge peak shift toward longer wavelengths due to the variation of the chlorophyll content and the *double-peak* feature observed on the derivative spectra when fluorescence effects are included. This result confirms laboratory experiments conducted in Zarco-Tejada et al. (2003) and later discussed in Le Maire et al. (2004).

This manuscript validated fluorescence extraction from airborne imagery using the *in-filling* method with comparisons to field-measured steady-state fluorescence (*Fs*) using the PAM-2100 instrument. In addition, to address potential structural effects on fluorescence retrievals from the airborne imagery, such as the influence of tree LAI, extracted crown NDVI was shown to have no relationship with crown fluorescence extracted from the imagery ($r^2 = 0.05$), demonstrating the sensitivity of R757.5 and R760.5 nm bands to fluorescence and an absence of crown LAI influences. The consistency of airborne fluorescence retrievals from trees under water stress condition using the methods reported in the manuscript (higher *F* values on fully-irrigated compared to deficit watered trees) was assessed against crown temperature, another physiological indicator of water stress linked with fluorescence emission. Retrievals from the airborne imagery showed an inverse relationship between crown fluorescence and temperature, as expected in water stressed trees (lower *F* and higher *T* in water stressed trees). Fluorescence emission retrievals were also related with assimilation measures conducted in the field at the time of the airborne acquisitions.

The manuscript demonstrates that fluorescence retrievals from vegetation canopies can be conducted operationally using multispectral cameras of 1 nm FWHM bands centered at 757.5 and 760.5 nm, supported by inferences from a simulation study with FluorMOD model. The validated methods enable the generation of fluorescence images at 15 cm resolution acquired at 150 m above the ground for vegetation stress detection. A similar demonstration of operational feasibility of fluorescence retrievals with a suitable imaging spectrometer using the specific reflectance indices identified in the simulation study with FluorMOD as reported here remains to be done in future research.

Acknowledgements

References

Abadía, J., Morales, F., & Abadía, A. (1999). Photosystem II efficiency in low chlorophyll, iron-deficient leaves. *Plant Soil, 215*, 183—192.

Agati, G. (1998). Response of the in vivo chlorophyll fluorescence spectrum to environmental factors and laser excitation wavelength. *Pure and Applied Optics, 7*, 797—807.

Berni, J. A. J., Zarco-Tejada, P. J., Suárez, L., & Fereres, E. (2009). Thermal and narrow-band multispectral remote sensing for vegetation monitoring from an unmanned aerial vehicle. *IEEE Transactions on Geoscience and Remote Sensing, 47*(3), 722—738.

Björkman, O., & Powles, S. B. (1984). Inhibition of photosynthetic reactions under water stress: Interaction with light level. *Planta, 161*, 490—504.

Bradford, K. J., & Hsiao, T. C. (1982). Physiological responses to moderate water stress. In O. L. Lange, P. S. Nobel, C. B. Osmond, & H. Ziegler (Eds.), *Encyclopedia of plant physiology, N.S.Physiological plant ecology II: Water relations and carbon assimilation, Vol. 12B*. (pp. 263—324) Berlin Heidelberg New York: Springer.

Carter, G. A., Cibula, W. G., & Miller, R. L. (1996). Narrow-band reflectance imagery compared with thermal imagery for early detection of plant stress. *Journal of Plant Physiology, 148*, 515—522.

Carter, G. A., Freedman, A., Kebabian, P. L., & Scott, H. E. (2004). Use of a prototype instrument to detect short-term changes in solar-excited leaf fluorescence. *International Journal of Remote Sensing, 25*, 1779—1784.

Carter, G. A., Jones, J. H., Mitchell, R. J., & Brewer, C. H. (1996). Detection of solar-excited chlorophyll a fluorescence and leaf photosynthetic capacity using a Fraunhofer line radiometer. *Remote Sensing of Environment, 55*, 89—92.

Carter, G. A., Theisen, A. F., & Mitchell, R. J. (1990). Chlorophyll fluorescence measured using the Fraunhofer line-depth principle and relationship to photosynthetic rate in the field. *Plant, Cell and Environment, 13*, 79—83.

Evain, S., Flexas, J., & Moya, I. (2004). A new instrument for passive remote sensing: 2. Measurement of leaf and canopy reflectance changes at 531 nm and their relationship with photosynthesis and chlorophyll fluorescence. *Remote Sensing of Environment, 91*, 175—185.

Fereres, E., & Soriano, M. (2007). Deficit irrigation for reducing agricultural water use. *Journal of Experimental Botany, 58*, 147—159.

Flexas, J., Briantais, J. -M., Cerovic, Z., Medrano, H., & Moya, I. (2000). Steady-state and maximum chlorophyll fluorescence responses to water stress in grapevine leaves: A new remote sensing system. *Remote Sensing of Environment, 73*, 282—297.

Flexas, J., Escalona, J. M., Evain, S., Gulias, J., Moya, I., Osmond, C. B., et al. (2002). Steady-state chlorophyll fluorescence (Fs) measurements as a tool to follow variations of net CO2 assimilation and stomatal conductance during water-stress in C-3 plants. *Physiologia Plantarum, 114*(2), 231—240.

Flexas, J., Escalona, J. M., & Medrano, H. (1999). Water stress induces different levels of photosynthesis and electron transport rate regulation in grapevines. *Plant Cell and Environment, 22*, 39—48.

Gao, B. C. (1996). NDWI—A normalized difference water index for remote sensing f vegetation liquid water from space. *Remote Sensing of Environment, 58*, 257—266.

Hsiao, T. C., Fereres, E., Acevedo, E., & Henderson, D. W. (1976). *Water stress and dynamics of growth and yield of crops. Water and Plant life: Problems and modern approaches.* (pp.): Springer.

Idso, S. B., Jackson, R. D., Pinter, P. J., Reginato, R. J., & Hatfield, J. L. (1981). Normalizing the stress-degree-day parameter for environmental variability. *Agricultural and Forest Meteorology, 24*, 45—55.

Idso, S. B., Jackson, R. D., & Reginato, R. J. (1978). Extending the "degree day" concept of phenological development to include water stress effects. *Ecology, 59*, 431—433.

Jackson, R. D., Idso, S. B., Reginato, R. J., & Ehrier, W. L. (1977). Crop temperature reveals stress. *Crop Soils, 29*, 10—13.

Jackson, R. D., Idso, S. B., Reginato, R. J., & Pinter, P. J. (1981). Canopy temperature as crop water-stress indicator. *Water Resources Research, 17*, 1133—1138.

Jackson, R. D., & Pinter, P. J., Jr. (1981). Detection of water stress in wheat by measurement of reflected solar and emitted thermal IR radiation. *Spectral Signatures of Objects in Remote Sensing, Institut National de la Reserche Agronomique, Versalles, France* (pp. 399—406).

Krause, G. H., & Weis, E. (1984). Chlorophyll fluorescence as a tool in plant physiology. II. Interpretation of fluorescence signals. *Photosynthesis Researsch, 5*, 139—157.

Larcher, W. (1994). Photosynthesis as a tool for indicating temperature stress events. In E. D. Schulze & M. M. Caldwell (Eds.), *Ecophysiology of photosynthesis* (pp. 261—277). Berlin: Springer.

Le Maire, G., François, C., & Dufrêne, E. (2004). Towards universal broad leaf chlorophyll indices using PROSPECT simulated database and hyperspectral reflectance measurements. *Remote Sensing of Environment, 89*, 1—28.

Lichtenthaler, H. K. (1992). The Kautsky effect: 60 years of chlorophyll fluorescence induction kinetics. *Photosynthetica, 27*, 45—55.

Lichtenthaler, H. K., & Rinderle, U. (1988). The role of chlorophyll fluorescence in the detection of stress conditions in plants. *CRC Critical Reviews in Analytical Chemistry, 19*(Suppl. 1), 529—585.

Liu, L., Zhang, Y., Wang, J., & Zhao, C. (2005). Detecting solar-induced chlorophyll fluorescence from field radiance spectra based on the Fraunhofer line principle. *IEEE Transactions on Geoscience and Remote Sensing, 43*, 827—832.

Maier, S.W. (2000), Modeling the radiative transfer in leaves in the 300 nm to 2.5 μm wavelength region taking into consideration chlorophyll fluorescence—The leaf model SLOPE. *PhD Thesis—Technische Universität München (München)*, 124 pp.

Maier, S. W., Günther, K. P., & Stellmes, M. (2002). Remote sensing and modelling of solar induced fluorescence. *1st Workshop on Remote Sensing of Solar Induced Vegetation Fluorescence, Noordwijk, Netherlands.*

Maier, S. W., Lüdeker, W., & Günther, K. P. (1999). SLOP: A revised version of the stochastic model for leaf optical properties. *Remote Sensing of the Environment, 68*(3), 273—280.

McFarlane, J. C., Watson, R. D., Theisen, A. F., Jackson, R. D., Ehrler, W. L., Pinter, P. J., Jr., et al. (1980). Plant stress detection by remote measurement of fluorescence. *Applied Optics, 19*, 3287—3289.

Meroni, M., Picchi, V., Rossini, M., Cogliati, S., Panigada, C., Nali, C., et al. (2008). Leaf level early assessment of ozone injuries by passive fluorescence and PRI. *International Journal of Remote Sensing, 29*, 17,5409—5422.

Meroni, M., Rossini, M., Picchi, V., Panigada, C., Cogliati, S., Nali, C., et al. (2008). Assessing steady-state fluorescence and PRI from hyperspectral proximal sensing as early indicators of plant stress: the case of ozone exposure. *Sensors, 8*, 1740—1754.

Miller, J.R., Berger, M., Alonso, L., Cerovic, Z., Goulas, Y., Jacquemoud, S., et al. s(2004), Progress on the development of an integrated canopy fluorescence model, 2003—International Geoscience and Remote Sensing Symposium, IGARSS'03, pp. 601–603 Vol.1, ISBN 0-7803-7929-2-0-7803-7930-6, Toulouse (France), 21—25 / 7 /2004.

Morales, F., Abadía, A., & Abadía, J. (1991). Chlorophyll fluorescence and photon yield of oxygen evolution in iron-deficient sugar beet (*Beta vulgaris* L.). *Plant Physiology, 97*, 886—893.

Morales, F., Abadía, A., & Abadía, J. (1998). Photosynthesis quenching of chlorophyll fluorescence and thermal energy dissipation in iron-deficient sugar beet leaves. *Australian Journal of Plant Physiology, 25*, 403—412.

Morales, F., Abadía, A., & Abadía, J. (2006). Photoinhibition and photoprotection under nutrient deficiencies, drought and salinity. In B. Demmig-Adams, W. W. AdamsIII, & A. K. Mattoo (Eds.), *Photoprotection, photoinhibition, gene regulation, and environment* (pp. 65—85). The Netherlands: Springer.

Morales, F., Belkhodja, R., Abadía, A., & Abadía, J. (2000). Photosystem II efficiency and mechanism of energy dissipation in iron-deficient, field grown pear trees (*Pyrus communis* L.). *Photosynthesis Research, 63*, 9—21.

Moya, I., Camenen, L., Evain, S., Goulas, Y., Cerovic, Z. G., Latouche, G., et al. (2004). A new instrument for passive remote sensing 1. Measurements of sunlight-induced chlorophyll fluorescence. *Remote Sensing of Environment, 91*, 186—197.

Papageorgiou, G. (1975). Chlorophyll fluorescence: An intrinsic probe of photosynthesis. In Govindjee (Ed.), *Bioenergetics of photosynthesis* (pp. 319—371). New York: Academic Press.

Pedrós, R., Jacquemoud, S., Goulas, Y., Louis, J., & Moya, I. (2004). A new leaf fluorescence model. *2nd International Workshop on Remote Sensing of Vegetation Fluorescence, 17—19 Nov. Montreal, Canada.*

Pedrós, R., Moya, I., Goulas, Y., & Jacquemoud, S. (2008). Chlorophyll fluorescence emission spectrum inside a leaf. *Photochemical and Photobiological Reviews, 7*(4), 498—502.

Peguero-Pina, J. J., Morales, F., Flexas, J., Gil-Pelegrín, E., & Moya, I. (2008). Photochemistry, remotely sensed physiological reflectance index and de-epoxidation state of the xanthophyll cycle in *Quercus coccifera* under intense drought. *Oecologia, 156*(1), 1—11.

Peñuelas, J., Filella, I., Biel, C., Serrano, L., & Save, R. (1993). The reflectance at the 950–970 nm region as an indicator of plant water status. *International Journal of Remote Sensing, 14*, 1887—1905.

Peñuelas, J., Llusia, J., Piñol, J., & Filella, I. (1997). Photochemical reflectance index and leaf photosynthetic radiation-use-efficiency assessment in Mediterranean trees. *International Journal of Remote Sensing, 18*, 2863—2868.

Pérez-Priego, O., Zarco-Tejada, P. J., Sepulcre-Cantó, G., Miller, J. R., & Fereres, E. (2005). Detection of water stress in orchard trees with a high-resolution spectrometer through chlorophyll fluorescence *in-filling* of the O2-A band. *IEEE Transactions on Geoscience and Remote Sensing, 43*, 2860—2869.

Rock, B. N., Vogelmann, J. E., Williams, D. L., Vogelmann, A. F., & Hoshizaki, T. (1986). Remote detection of forest damage. *Biosciencie, 36*, 439—455.

Schreiber, U., & Bilger, W. (1987). Rapid assessment of stress effects on plant leaves by chlorophyll fluorescence measurements. In J. D. Tenhunen, & E. M. Catarino (Eds.), *Plant response to stress* (pp. 27—53). Berlin, Germany: Springer-Verlag.

Schreiber, U., Bilger, W., & Neubauer, C. (1994). Chlorophyll fluorescence as a non-intrusive indicator for rapid assessment of in vivo photosynthesis. In E. D. Schulze, & M. M. Caldwell (Eds.), *Ecophysiology of photosynthesisEcological Studies, Vol 100.* (pp. 49—70) Berlin Heidelberg New York: Springer.

Sepulcre-Cantó, G., Zarco-Tejada, P. J., Jiménez-Muñoz, J. C., Sobrino, J. A., de Miguel, E., et al. (2006). Within-field thermal variability detection as function of water stress in *Olea europaea* L. orchards with high spatial remote sensing imagery. *Agricultural and Forest Meteorology, 136*, 31—44.

Sepulcre-Cantó, G., Zarco-Tejada, P. J., Jiménez-Muñoz, J. C., Sobrino, J. A., Soriano, M. A., Fereres, E., et al. (2007). Monitoring yield and fruit quality parameters in open-canopy tree crops under water stress. Implications for ASTER. *Remote Sensing of Environment, 107*, 455—470.

Slatyer, J. O. (1967). *Plant–water relationships.*New York: Academic press 366 pp.

Smith, G. M., & Milton, E. J. (1999). The use of the empirical line method to calibrate remotely sensed data to reflectance. *International Journal of Remote Sensing, 20*, 2653—2662.

Soukupová, J., Cséfalvay, L., Urban, O., Kosvancová, M., Marek, M., Rascher, U., & Nebdal, L. (2008). Annual variation of the steady-state chlorophyll fluorescence emission of evergreen plants in temperate zone. *Functional Plant Biology, 35*, 63—76.

Suárez, L., Zarco-Tejada, P. J., Berni, J. A. J., González-Dugo, V., & Fereres, E. (2009). Modelling PRI for water stress detection using radiative transfer models. *Remote Sensing of Environment, 113*, 730—744.

Suarez, L., Zarco-Tejada, P. J., Sepulcre-Cantó, G., Pérez-Priego, O., Miller, J. R., & Jiménez-Muñoz, J. C. (2008). Assessing canopy PRI for water stress detection with diurnal airborne imagery. *Remote Sensing of Environment, 112*, 560—575.

Thenot, F., Méthy, M., & Winkel, T. (2002). The photochemical reflectance index (PRI) as a water-stress index. *International Journal of Remote Sensing, 23*(23), 5135—5139.

Verhoef, W. (2005). Extension of SAIL to model solar-induced canopy fluorescence spectra. *2nd International Workshop on Remote Sensing of Vegetation Fluorescence, 17–19 Nov. 2004, Montreal, Canada.*

Wolfe, D. W., Fereres, E., & Voss, R. E. (1983). Growth and yield response of two potato cultivars to various levels of water applied. *Irrigation Science, 3*, 211—222.

Zarco-Tejada, P. J., Miller, J. R., Mohammed, G. H., & Noland, T. L. (2000). Chlorophyll fluorescence effects on vegetation apparent reflectance: I. Leaf-level measurements and simulation of reflectance and transmittance spectra. *Remote Sensing of Environment, 74*(3), 582—595.

Zarco-Tejada, P.J., Miller, J.R., Haboudane, D., Tremblay, N., Apostol, S. (2004). Detection of chlorophyll fluorescence in vegetation from airborne hyperspectral CASI imagery in the red edge spectral region. 2003—International Geoscience and Remote Sensing Symposium, IGARSS'03, pp. 598–600 Vol.1, ISBN 0-7803-7929-2–0-7803-7930-6, Toulouse (France), 21–25/7/2004.

Zarco-Tejada, P. J., Miller, J. R., Mohammed, G. H., Noland, T. L., & Sampson, P. H. (2000). Chlorophyll fluorescence effects on vegetation apparent reflectance: II. Laboratory and hyperspectral airborne experiments. *Remote Sensing of Environment, 74*(3), 596—608.

Zarco-Tejada, P. J., Miller, J. R., Pedrós, R., Verhoef, W., & Berger, M. (2006). FluorMODgui V3.0—A graphic user interface for the leaf and canopy simulation of chlorophyll fluorescence. *Computers & Geosciences, 32*, 577—591.

Zarco-Tejada, P. J., Pushnik, J., Dobrowski, S., & Ustin, S. L. (2003). Steady-state chlorophyll a fluorescence detection from canopy derivative reflectance and double-peak red-edge effects. *Remote Sensing of Environment, 84*(2), 283—294.